Contributed paper

OPTO-ELECTRONICS REVIEW **11**(2), 143–149 (2003)

Analysis of VLWIR HgCdTe photodiode performance

J. WENUS*, J. RUTKOWSKI, and A. ROGALSKI

Institute of Applied Physics, Military University of Technology,
2 Kaliskiego St., 00-908 Warsaw, Poland

The performance of very long wavelength infrared (VLWIR) HgCdTe photodiodes at temperatures ranging from 77 K up to 150 K is presented. The effect of inherent and excess current mechanisms on quantum efficiency and dynamic resistance-area RA product is analysed. Different methods of determining the ideality factor are shown and among them the one based on the use of RA product versus bias voltage proves to be the most reliable. At higher temperatures, however, the calculated ideality factor does not give any useful information about the nature of the p-n junction current due to significant influence of the series and shunt resistances. A comparison of the experimental data with the results of analytical and numerical calculations shows that the photodiodes with cut-off wavelength up to 14.5 μm are diffusion-limited at temperatures exceeding 100 K.

Keywords: HgCdTe photodiodes, heterostructure, ideality factor, R_0A product, quantum efficiency.

1. Introduction

HgCdTe is well established as a variable gap semiconductor for fabricating of high-sensitivity detectors over a wide infrared (IR) spectral range. A significant progress in HgCdTe material and detector technology enables the fabrication of infrared detectors operating in very long wavelength infrared (VLWIR) range λ_c = 14–17 μm). The back-side-illuminated mesa P-on-n double-layer heterojunction (DLHJ) has become the most widely applicable for use in hybrid VLWIR focal plane arrays since the larger gap reduces the dark current contribution from the p-type material [1]. Although a number of growth techniques are used for device development, most detector material continues to be grown by liquid phase epitaxy (LPE) because of the combination of large wafer area with consistently high material quality [2]. There are, however, significant problems with the proper characterization of the photodiodes because of very small energy gap (E_g < 0.1 eV). Within this range of E_g the precision of determining the material composition is very important, because small fluctuations in temperature can cause considerable shift in the cut-off wavelength of the photodiode. Another inconvenience is the necessity to apply small base layer doping concentration to avoid tunneling currents. The low level of doping entails additional problems with the increase in series and contact resistances as well as in the surface leakage currents, especially in case of improper surface passivation [3]. Next phenomenon characteristic for the DLHJ is the formation of a valence-band barrier and its negative or positive influence on detector parameters.

In this work, the mesa isolated devices based on DLHJ grown by LPE, with active region composition of x = 0.2, are investigated. The measurements of current-voltage (I-V), dynamic resistance-voltage (R-V) and capacity-voltage (C-V) characteristics are performed. The dominant dark current mechanisms impacting the photodiodes performance are specified by the analysis of the I-V and R-V curves for low reverse and forward biases and different temperatures of operation. Due to low values of dynamic resistance (often comparable to series resistance), there are difficulties with determining the basic photodiode parameters, such as quantum efficiency and R_0A product. On account of that, the following relationships were analysed:

- influence of series resistance R_s and shunt resistance R_{sh} on junction parameters,
- the sources of the resistances and possibilities of their reduction,
- ideality factor n as a function of temperature and surface passivation,
- surface recombination velocity depending on the method of passivation,
- significance of the valence-band barrier and lateral effects.

The experimental data are confirmed by theoretical predictions based on analytical calculations as well as numerical simulations. Photodiodes with cut-off wavelengths up to 14.5 μm and performance determined by diffusion effects up to 100 K are demonstrated.

2. Device fabrication

The DLHJ structures used in fabrication of $Hg_{1-x}Cd_xTe$ photodiodes were grown on CdZnTe substrates by liquid phase epitaxy (LPE). The n-type base layer with composition x = 0.2 was deliberately doped with indium at a level

*e-mail: j.wenus@wat.edu.pl

of about 5×10^{14}–1×10^{15} cm^{-3} and grown from Te-rich melt at approximately 480°C. The thickness of the film was about 17 μm. A 1–2 μm thick cap layer, arsenic doped (10^{17} cm^{-3}), with a wide band-gap (x = 0.24) was grown in second LPE process from Hg-rich melt at 360°C. The standard photolithographic techniques and etching in a 5% Br:ethylene glycol were used for the fabrication of mesa structures.

Electric contacts were made by thermal evaporation of gold to P-type cap layer and indium to n-type active material. Additional ion milling was performed prior to the indium deposition, to improve the n-type contact.

Two different surface passivation methods were conducted: CdTe and ZnS deposition on clear HgCdTe surface by thermal evaporation under high vacuum conditions.

The current-voltage characteristics were measured in liquid nitrogen cooled cryostat system for the temperature range between 77 K and 150 K. The diodes were characterized by I-V and C-V measurements under dark conditions. All the electrical measurements were done by computer controlled digital programmable equipment.

3. Results and discussion

3.1. Electrical measurements

A typical measured current-voltage plot and corresponding dynamic impedance of a 400 μm diameter diode at 77 K is shown in Fig. 1. One can easily distinguish two linear regions in the I-V plot. Under forward bias conditions, the resistance of the photodiode is determined by the series resistance – R_s. Two main components contribute to the resistance: the n-type base layer and the electric contacts. In the reverse bias region, however, the influence of shunt resistance – R_{sh}, which is usually similar to the R_{max}-value, predominates. The main source of the shunt resistance is a surface leakage current connected with the passivation of the junction. Both the series and the shunt resistances are comparable to the zero-bias junction resistance – R_0. For the presented photodiode the above-mentioned values are as follows: R_s = 29 Ω, R_{sh} = 552 Ω, R_{max} = 600 Ω, and R_0 = 286 Ω. The last value gives the zero-bias resistance-area product $R_0A \approx 0.4\ \Omega\,\text{cm}^2$.

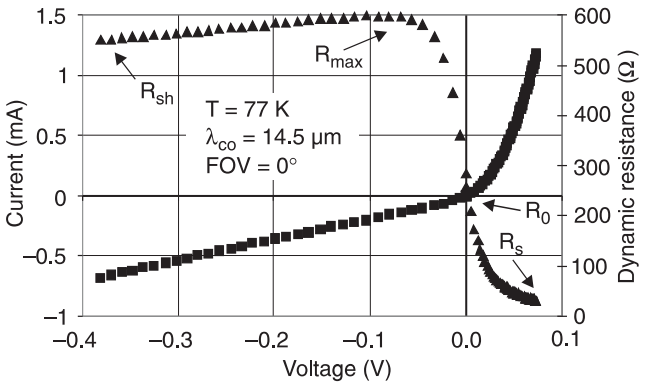

Fig. 1. Typical current-voltage and dynamic resistance-voltage plots for a DLHJ photodiode.

All the characteristic resistances of a photodiode differ depending on the way of passivation of the junction surface, and the method of the electric contact deposition. Figure 2 shows several different plots of dynamic resistance-area product as a function of bias voltage for photodiodes with the same junction diameter equal to 400 μm. The curves marked by numbers 1, 2, and 3 correspond to diodes with increasing contact resistance, respectively. The influence of the resistance is clearly visible under the forward bias conditions and it makes it difficult to precisely determine the R_s value (curve 3). On the other hand, the reverse-biased diodes exhibit sometimes a strong tunneling effect (curves 4 and 5). The tunneling currents are usually caused by the improper passivation of the p-n junction surface. The shunt resistance R_{sh} is then practically indeterminate and the R_{max} value is getting closer to the zero-bias resistance R_0.

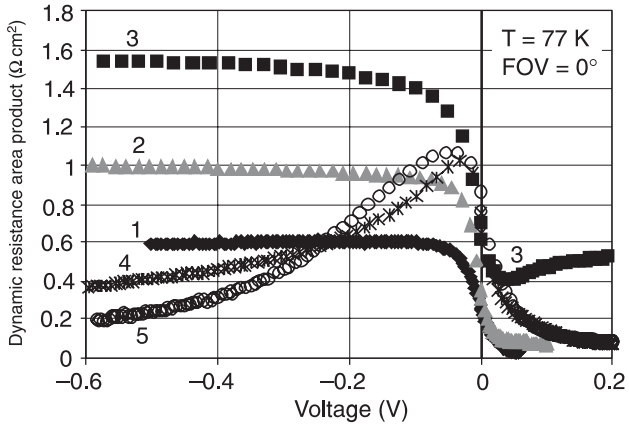

Fig. 2. R-V plots for photodiodes made from the same material by different methods.

In case of small R_s value, the area of the p-n junction has also an influence on the shape of the R-V characteristics. Figure 3 shows three dynamic resistance-voltage plots for photodiodes with different junction radius (1–200 μm, 2–90 μm, 3–65 μm). The visible drop in the RA product with decreasing junction area is caused by the influence of a surface leakage effect and lateral collection of charge carriers. Because of these effects, the series resistance R_s has minor impact on photodiodes with smaller junction dimensions.

In order to obtain additional information about the heterojunction, capacitance voltage (C-V) measurements were performed (Fig. 4). The linear dependence $1/C^2$ as a function of voltage is the evidence of abrupt character of the junction. The concentration of donors obtained from the slope of the plot is with good agreement with the N_d value received from Hall effect measurements carried out on the base layer material. The disturbance, which can be seen in Fig. 4 near zero-bias, is probably a result of small valence-band barrier on the heterojunction. The barrier pre-

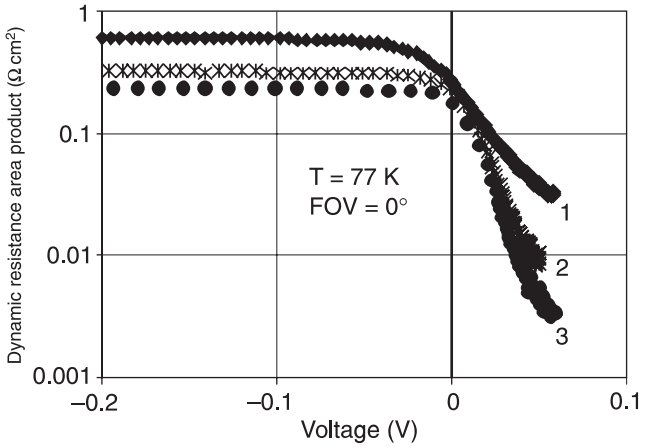

Fig. 3. R-V plots for photodiodes with different junction radius (1–200 μm, 2–90 μm, 3–65 μm).

vents the charge carriers from flowing through the junction and thus, the capacitance increases. A reverse bias reduces the potential barrier and therefore the curve in Fig. 4 straightens. Extension of the linear part of the curve gives at the intersection with voltage axis the V_D value approximately equal to the energy gap of the base material (in eV).

More thorough analysis of the current-voltage characteristics is necessary to specify the current mechanisms which determine the performance of a VLWIR HgCdTe photodiode. Figure 5 shows a natural logarithm of the photodiode current as a function of applied voltage. Circles on this figure indicate the experimental results. Assuming, that the I-V plot is consistent with the Schockley equation: $I = I_s[\exp(qV/nkT) - 1]$ (where I_s is the saturation current, k is the the Boltzmann constant, q is the electron charge, and T is the absolute temperature) one can obtain the ideality factor n, which determines the dominant carrier transport mechanism. The factor is usually obtained from the slope of the linear dependence of $ln(I)$ on forward bias voltage [4,5]. In such case the Schockley equation converts to: $ln(I) = ln(I_s) + qV/nkT$. The value $n = 1$ indicates minority carrier diffusion, while $n = 2$ is obtained when generation and recombination of electron-hole pairs in the photodiode depletion region determines the forward dark current.

Proper assessment of the ideality factor, directly from experimental results, is possible only when there is no strong influence of the series resistance and shunt resistance on the shape of I-V curve of a photodiode. Under forward-bias conditions the R_s value is particularly important, because the voltage drop on the series resistance is getting more significant. Thus, for VLWIR photodiodes the following equation should be used to determine the n value

$$\ln(I) = \ln(I_s) + \frac{q(V - IR_s)}{nkT}. \qquad (1)$$

It is not always possible to precisely determine the series resistance from the experimental I-V curves and that is why a method of selection of the R_s was employed to obtain a linear dependence of $ln(I)$ on forward bias voltage.

Figure 5 shows a theoretical fit to the experimental results (black solid curve) with the factor $n = 1.33$ and the saturation current $I_s = 2.76\times10^{-6}$ A, obtained by the method described earlier. It is clearly seen that the fit is far from the experimental points. The reason for that is connected with strong influence of the R_s and R_{sh} values, which were not taken into consideration. The second fit (grey solid line) was plotted assuming a model of a photodiode consisted of an ideal p-n junction (with I-V dependence characterized by the black curve), serial resistance R_s and parallel (shunt) resistance R_{sh}. Such a model, on the other hand, gives an excellent fit to the results of measurements. The introduction of the R_{sh} is necessary, because in most cases it reduces the junction resistance, even near the zero-bias.

The ideality factor n and the saturation current I_s can be used to determine a theoretical value of the zero-bias resistance of the photodiode – R_{0t}, using a simple formula: $R_{0t} = nkT/qI_s$. The R_{0f} parameter calculated in this way, after taking into account the R_s and R_{sh} resistances, is similar to the measured value – R_0. Table 1 gives examples of the parameters obtained from the analysis of current-voltage characteristics of different photodiodes based on the same heterostructure. An interesting effect is that the experimental zero-bias resistance – R_0 is always higher than the R_{0f} value, obtained from the fitting. Apart from the precision of

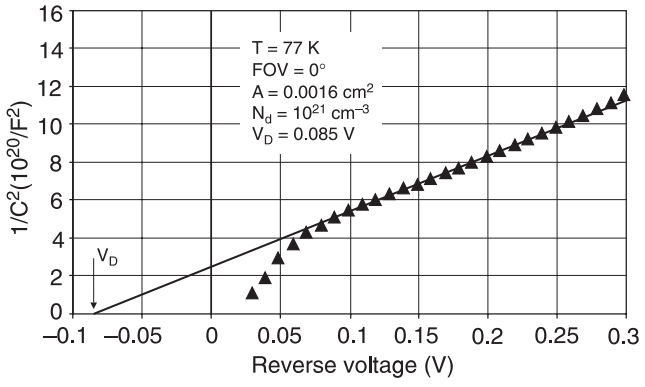

Fig. 4. Reciprocal of squared capacitance as a function of reverse bias voltage for a DLHJ photodiode.

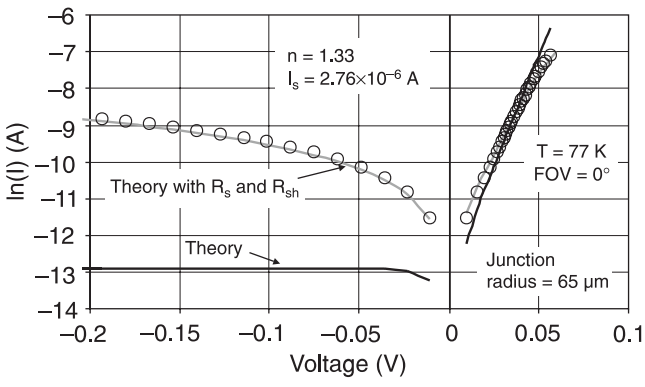

Fig. 5. Theoretical fit to the experimental results of I-V measurements.

Table 1. Parameters of different VLWIR DLHJ photodiodes.

Sample	n	I_s (A)	R_s (Ω)	R_{max}/R_{sh}	R_{0t}	R_{0f}	R_0	Additional information
EL-2e	1.33	2.76×10^{-6}	9	1400	3196	982	1050	junction radius = 65 μm
E-d6	1.41	1.33×10^{-5}	23	550	703	333	370	square 400×400 μm^2
EN-1b	1.89	2.04×10^{-5}	16	2500	614	510	600	square 400×400 μm^2
E-d21d	1.48	1.14×10^{-5}	73	4500	861	795	750	square 300×300 μm^2; high R_s and R_{sh}
E-d18f	2.37	2.32×10^{-5}	45	1400	678	502	495	square 400×400 μm^2; high R_s value
E-d14c	2.93	3.77×10^{-5}	50	2000	516	461	495	square 400×400 μm^2; high R_s value
EA-29d	5.71	5.19×10^{-5}	42	1400/905	730	523	600	junction radius = 200 μm; tunneling
EB-28c	4.50	3.46×10^{-5}	45	1400/950	863	579	700	junction radius = 200 μm; tunneling

determining the fitting parameters, the reason of the difference can be also connected with a potential barrier, which can appear at the heterostructure [6] and this phenomenon is not considered in the analytical calculations.

An ideality factor of 1.33 was determined from the fit to the best I-V characteristics, indicating that these devices are almost diffusion limited at liquid nitrogen temperature. The increase in series resistance entails also an increase in the ideality factor, even over 2, but it cannot be interpreted as stronger influence of the generation-recombination current, which will be proved later. If tunneling currents determine the junction resistance, the ideality factor exceeds the value of 2 considerably. In most cases, the n-value increases with the increase in temperature. Such behaviour is inexplicable from the physical point of view and can be explained simply as a result of the increase in R_s/R_0 ratio.

In higher temperatures, when the ratio is almost unity, determining the ideality factor from the current-voltage plot is practically impossible. In such cases another method of obtaining the n-value, based on the use of dynamic resistance versus bias voltage, is more reliable. The dynamic resistance can be calculated from the I-V plot according to the formula: $R = (dI/dV)^{-1}$. Assuming, that the current-voltage dependence is consistent with the Schockley equation, we can obtain the following expression

$$R = \frac{nkT}{I_s q}\exp\left(-\frac{qV}{nkT}\right) = R_0\exp\left(-\frac{qV}{nkT}\right). \qquad (2)$$

A natural logarithm performed on this formula gives a linear dependence

$$\ln(R) = \ln(R_0) - \frac{qV}{nkT}. \qquad (3)$$

In practice, however, the dynamic resistance-voltage plot has a linear character only in limited range, where there is no strong influence of the R_s and R_{sh}. With increasing temperature the range is shifting to the reverse bias voltages, what can be seen in Fig. 6 in the area outlined by a broken line.

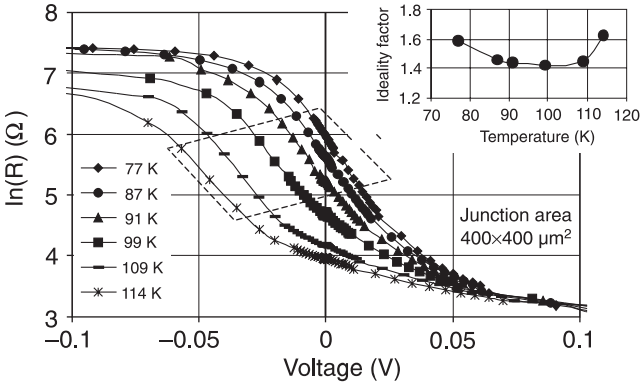

Fig. 6. Dynamic resistance as a function of bias voltage for different temperatures of operation.

The ideality factor n decreases from the value of 1.6 to 1.4 as the temperature grows from 77 K up to 100 K. The growth indicates minor significance of the generation-recombination currents in higher temperatures. On the other hand, the n-value increases rapidly for temperatures exceeding 110 K. This effect is connected with too big influence of the series and shunt resistances, which are getting comparable to the measured value of R_0. Thus, the ideality factor obtained from the *ln(R)-V* dependences at higher temperatures does not give any useful information about the nature of the current flowing through the p-n junction. This conclusion can be further confirmed by the results shown in Fig. 7.

The grey solid line in Fig. 7 represents analytical calculations of the R_0A product, where the current is determined only by diffusion of charge carriers in the n-type active layer and the lifetime of the carriers is governed by the Auger and radiative recombination effects. The square points are taken directly from the I-V measurements. It is clear, that the series resistance affects the R_0A value at temperatures above 110 K. At lower temperatures of operation the shunt resistance has more significant influence on the parameter. The dotted points in Fig. 7 reflect the experimental results after taking into account the values of R_s and R_{sh}. The comparison with the theoretical line shows, that the

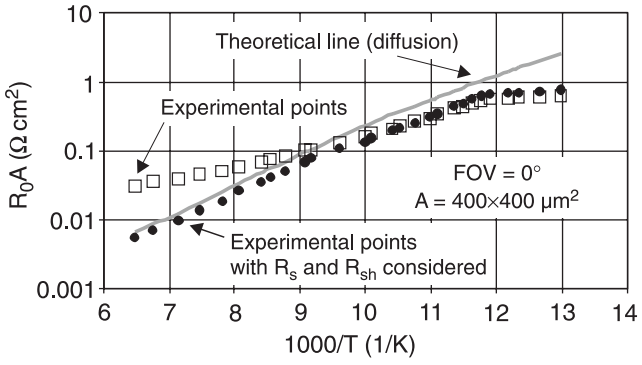

Fig. 7. Comparison of the theoretical and experimental R_0A dependencies on reciprocal temperature.

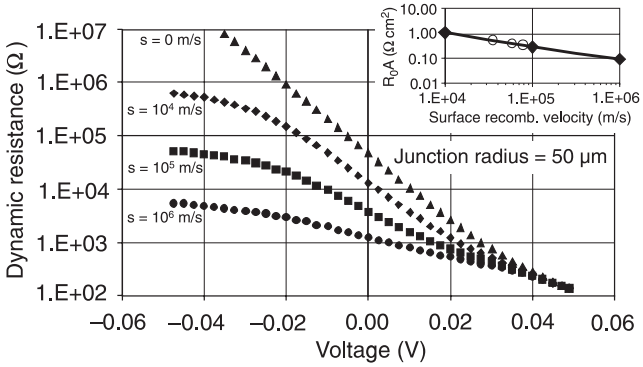

Fig. 9. Simulated R-V plots for photodiodes with different surface recombination velocities.

photodiode is almost diffusion limited down to 100 K, what is with good agreement with the results shown previously.

The value of the shunt resistance is determined by surface leakage currents, which depend on the method of the p-n junction passivation. To prove that, the measurements of the R_0A product as a function of the junction radius were performed for photodiodes based on the same heterostructure, but with different surface treatment. The three lines in Fig. 8 correspond to photodiodes without passivation, passivated with CdTe and ZnS.

The linear character of the dependences of the $(R_0A)^{-1}$ on the reciprocal junction radius indicates that the device parameters are determined by the surface recombination rather than by lateral effects. Comparison of the slopes of the plots with the following equation

$$\frac{1}{R_0A} = \frac{1}{R_0A_{1D}}\left(1+\frac{L_c}{r}\right)^2 + \frac{2qn_iws}{V_{bi}r}, \qquad (4)$$

enables obtaining the surface recombination velocities s, and the intersection with vertical axis gives the one-dimensional R_0A_{1D} product [7]. The other parameters in the equation are as follows: L_c is the lateral collection length, q is the electron charge, n_i is the intrinsic carrier concentration, w is the depletion region width, and V_{bi} is the built-in voltage. The lowest surface recombination velocity is observed for photodiodes without any passivation, while CdTe usually doubles the velocity and ZnS makes it three times higher. The one-dimensional R_0A_{1D} product obtained from the above plots is about 2 Ω cm² regardless of the passivation method, what is with good agreement with theoretical value.

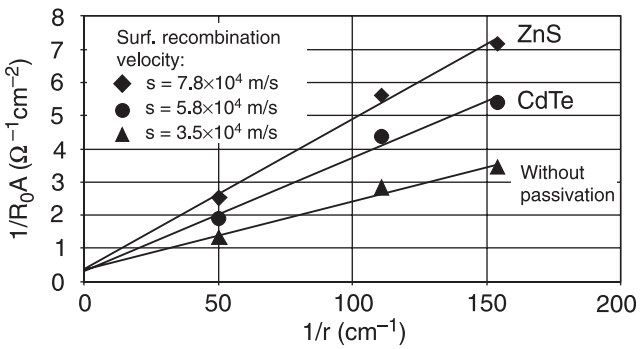

Fig. 8. Reciprocal R_0A product as a function of reciprocal junction radius for photodiodes with different surface passivation.

In order to confirm the results presented in Fig. 8, numerical simulations were performed for a photodiode with junction radius equal 50 μm and surface recombination velocity varying from 0 to 10^6 m/s. Figure 9 shows the dependence of calculated R-V plots on the magnitude of the recombination. The dynamic resistance near zero-bias decreases with the increase in the velocity of the recombination. Experimental values of the R_0A product are consistent with the results of simulations and they are presented in Fig. 9 as open circles.

The slope of the linear range of R-V plot decreases with increasing velocity of the surface recombination, which means that the ideality factor increases as well. The n-value calculated accordingly to the results presented in Fig. 9 varies from 1 for the case without the recombination, through 1.18, 1.70, and 3.35 for the recombination velocities of 10^4, 10^5, and 10^6 m/s respectively. Therefore the experimental ideality factors higher than 1 might be connected with the surface recombination rather than with the generation-recombination currents in the junction depletion region. This conclusion shows, that it is necessary to consider the shunt resistance, which is due to the surface recombination, to obtain a reliable value of the ideality factor. Thus, the discrepancies between the individual values of n in Table 1 can be, among other things, caused by the different surface passivation.

3.2. Optical measurements

Transmission measurements of $Hg_{1-x}Cd_xTe$ material at room temperature are combined with processed material detector spectral measurements at cryogenic temperatures to extract the material x value. A Fourier transform infrared

spectrometer is used to measure the transmission of the layer versus wavelength, yielding material x value and thickness information. Following $Hg_{1-x}Cd_xTe$ detector processing, the spectral response and quantum efficiency of the detector is measured. The modelled and measured quantum efficiencies versus wavelength are displayed in Fig. 10 for the cut-off wavelength λ_c = 14.5 μm at 77 K. The measured HgCdTe active layer thickness and the value of λ_c, are the input parameters to the model. The x_{opt} value is a fitting parameter that best replicates the shape of the measured quantum efficiency of the detector depending on the wavelength of incident radiation [8]. An x_{opt} = 0.202 was extracted from the quantum efficiency versus wavelength displayed in Fig. 10. The energy-gap corresponding to this composition is 0.08 eV, what agrees with the previously shown value of V_D (Fig. 4).

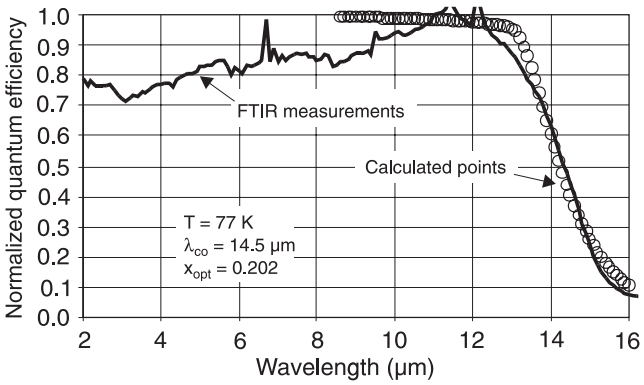

Fig. 10. Measured and calculated normalised quantum efficiency of a VLWIR photodiode.

Because of a large number of factors influencing the measured quantum efficiency of a VLWIR photodiode (absorption coefficient, active layer thickness, lateral collection, diffusion length, valence band barrier, series resistance) the value obtained in usual conditions, i.e., for zero-bias voltage, is not entirely reliable. Much more information can be received from the measurements performed as a function of applied voltage. Figure 11 presents the normalized quantum efficiency for three different photodiodes based on the same heterostructure.

The bias dependence of the quantum efficiency for three types of barriers (small – curve 1, higher – curve 2 and the highest – curve 3) have been determined and shown in Fig. 11. The results were also verified by numerical simulations, which show that the height of the barrier depends directly on the location of the p-n junction within the heterostructure and it grows when the junction is shifted towards the wider-gap region [9,10]. In practice, the control of the junction placement is carried out by a selection of appropriate parameters of annealing (temperature and time) in Hg vapours. The annealing process must be performed carefully to avoid the excessive interdiffusion at the heterojunction.

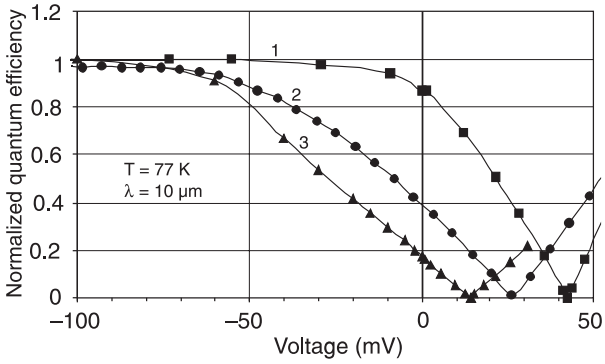

Fig. 11. Normalised quantum efficiency for three photodiodes with different potential barriers at the heterojunction.

All the measured values of quantum efficiency showed a drop near the zero bias voltage but the effect was much more significant for the diodes with higher potential barriers (curves 2 and 3). Applying of reverse bias reduces the valence-band barrier and therefore improves the quantum efficiency. At forward bias the photocurrent decreases to zero and then it changes its sign and suddenly increases due to domination of photoconduction effect over the photovoltaic signal. Photodiodes with the dependence of quantum efficiency on bias voltage similar to the one represented by the curve 1 in Fig. 11 exhibit the best performance.

4. Conclusions

The performance of VLWIR HgCdTe photodiodes has been analysed. It was found that the I-V and R-V characteristics are difficult to explain by a simple p-n junction model at liquid nitrogen temperature because the R_0, R_s, and R_{max} resistances are comparable to each other. The ideality factor varies from 1 to several depending on the surface treatment. The increase in n can be caused by different mechanisms: generation-recombination current in the depletion region, surface recombination or tunneling. Proper determining of the ideality factor requires taking into consideration the series and shunt resistances, especially at higher temperatures. When the impact of the R_s and R_{sh} is particularly significant, it is better to determine the n-value from the linear slope of the $ln(R)$ dependence on bias voltage rather than from the I-V curve.

In order to achieve a full explanation of the observed phenomena, additional measurements and analysis of the temperature dependencies are necessary. The most reliable information about the dominating effects can be obtained from the relationship between dynamic resistance and bias voltage, measured for several different temperatures of operation. The analysis of photocurrent as a function of applied voltage should be performed to estimate the quantum efficiency and assess the significance of potential barrier at the heterojunction.

The best parameters were obtained for the photodiodes without passivation. The performance of passivated photo-

diodes was limited mainly by the surface recombination and the reduction was more significant for ZnS than for CdTe. Our results indicate that further improvements in the performance of the VLWIR DLHJ HgCdTe photodiodes can be achieved by better surface passivation.

Acknowledgment

This work was partially supported by the Polish State Committee for Scientific Research (KBN) (project No. 4T08A 03123).

References

1. M.B. Reine, "Photovoltaic detectors in HgCdTe", *Infrared Detectors and Emitters: Materials and Devices*, Chapt.12 edited by P. Capper and C.T. Elliott, Chapman and Hall, London, 2000.
2. A. Rogalski, K. Adamiec, and J. Rutkowski, *Narrow-Gap Semiconductor Photodiodes*, SPIE Optical Engineering Press, Bellingham, 2000.
3. H.R. Vydyanath and V. Nathan, "Materials and process issues in the fabrication of high performance VLWIR HgCdTe infrared detectors", *Opto-Electron. Rev*. **9**, 1–5 (2001).
4. Li Xiangyang, Zhao Jun, Lu Huiqing, Fang Jiaxiong, and Xia Yueyuan, "Forward current-voltage characteristics of HgCdTe p-on-n photodiodes", *Proc. SPIE* **3379**, 601–607 (1998).
5. G. Sarusi, A. Zemel, Ariel Sher, and D. Eger, "Forward tunneling current in HgCdTe photodiodes", *J. Appl. Phys.* **76**, 4420–4425 (1994).
6. J. Wenus and J. Rutkowski, "Influence of valence-band barriers in VLWIR HgCdTe P-on-n heterojunctions on photodiode parameters", *Physica Status Solidi (b)* **229**, 1093–1096 (2002).
7. M.H. Weiler and G.J. Tarnowski, "Characterization of HgCdTe P-on-n heterojunctjon photodiodes and their defects using variable-area test structures", *J. Electr. Materials* **26**, 635–642 (1997).
8. A.I. D'Souza, R.E. DeWames, P.S. Wijewarnasuriya, G. Hildebrandt, and J.M. Arias, "Current mechanisms in VLWIR $Hg_{1-x}Cd_xTe$ photodiodes", *J. Electr. Materials* **30**, 585–589 (2001).
9. J. Wenus, J. Rutkowski, and A. Rogalski, "Two-dimensional analysis of double-layer heterojunction HgCdTe photodiodes", *IEEE Transactions on Electron Devices* **48**, 1326–1332 (2001).
10. M.H. Weiler and M.B. Reine, "Effect of a valence-band barrier on the quantum efficiency and background-limited dynamic resistance of compositionally graded HgCdTe P-on-n heterojunction photodiodes", *J. Electr. Materials* **24**, 1329–1339 (1995).

Faculty of Physics Warsaw University of Technology
Institute of Applied Physics Military University of Technology
Committee on Electronics and Telecommunication of PAS
Polish Optoelectronics Committee of SEP

XVII SCHOOL ON OPTOELECTRONICS
PHOTOVOLTAICS – SOLAR CELLS and DETECTORS

Kazimierz Dolny, October 13–16, 2003

Solar Cells:

Photovoltaics in Poland and in the World
Silicon cells (c-Si, a-Si, poli-Si)
Polycrystalline cells ($CuInSe_2$, CdTe)
$A^{III}B^{V}$ cells
Organic cells
Photovoltaic modules and systems
Photovoltaic metrology

Detectors:

Fundamentals of detection (thermal and photon detectors)
Visible and UV detectors
Infrared detectors
Focal plane arrays
Systems of detection
Applications of detectors

ADDRESS FOR CORRESPONDENCE:

Andrzej Kubiaczyk
Faculty of Physics
Warsaw University of Technology
02–625 Warsaw
ul. Św. Andrzeja Boboli 8
FOTOWOLT
e-mail: fotowolt@if.pw.edu.pl

Deadline for abstract submission – June 30, 2003
http://www.if.pw.edu.pl/~fotowolt

